Tailoring Stepped Layered Titanates for Sodium-Ion Battery Applications

Wei Yin,[a] Juhyeon Ahn,[a] Gözde Barim,[a] Judith Alvarado[a] and Marca M. Doeff,[*a]

a) Energy Storage and Distributed Resources Division

Lawrence Berkeley National Laboratory

1 Cyclotron Road

Berkeley, CA 94720 USA

*mmdoeff@lbl.gov

Conspectus

Concerns about sustainability and supply-chain issues associated with lithium-ion batteries (LIBs) have led researchers and companies around the world to investigate alternative technologies. Of all the so-called "beyond LIBs", sodium-ion batteries (NIBs) are in the most advanced stage of development, and are being considered for grid storage applications as well as moderate-range electric vehicles. While graphite is the most commonly used anode material for LIBs, hard carbons are used in NIBs because sodium insertion into graphite does not occur to a useful extent. Other possibilities, based on cost and availability arguments, are titanates, which are generally denser than disordered carbons, meaning more material can be packed into a given volume, leading potentially to greater energy density. We have researched stepped layered titanates for use as anode materials, focusing on two types of structures. The first is "sodium nonatitanate" or NNT, with the composition $NaTi_3O_6(OH)\cdot 2H_2O$ having six $Ti^{4+}O_6$ octahedra joined together in steps to form layers with sodium ions and water in-between. The lepidocrocite-type titanate structure, contains zigzag layers (or steps one $Ti^{4+}O_6$ unit across). These exist in a wide range of compositions, and contain large exchangeable cations between the layers. An unusual feature of both NNT and the lepidocrocite titanates is the very low potentials (0.3–0.5V vs. Na^+/Na) at which they insert sodium. This makes them particularly attractive for anode applications. Another interesting feature is the ability to tailor the electrochemical properties by various modifications, such as heat-treatment to remove water and change the structure, introduction of vacancies, ion-exchange, surface modifications, and carbon coating or graphene wrapping, all of which alter the electrochemical properties. Finally, heterostructuring (interleaving titanate layers with carbon) results in new materials with different redox properties.

For all the titanates, the first cycle coulombic efficiency (C.E.) is very sensitive to the binder used in the electrode fabrication and the electrolyte used. Because sodium insertion occurs at such a low potential, some electrolyte and binder are irreversibly reduced during the first cycle to form a protective solid electrolyte interphase (SEI). In a full cell, it is important to maximize the C.E. because all the cyclable sodium must come from the cathode, so cells must be overbuilt to compensate for these losses. Proper selection of binder and electrolyte results in improved cycling performance and minimal first cycle losses. Finally, examples of full cells containing some of the materials under discussion are provided.

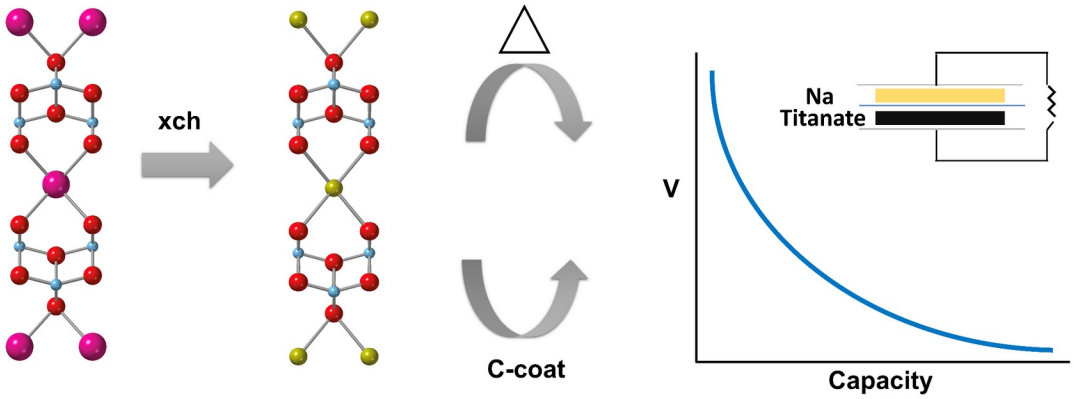

Biographies

Marca M. Doeff is a senior scientist and Deputy Division Director of the Energy Storage and Distributed Resources Division at Lawrence Berkeley National Laboratory (LBNL). She received her B.A. in Chemistry from Swarthmore College, Swarthmore PA in 1978 and a PhD in Inorganic Chemistry from Brown University in 1983. After postdoctoral work at U.C. Santa Barbara and U. C. Berkeley, she worked as a senior member of the technical staff at the Naval Ocean Systems Center in San Diego, CA, before joining LBNL in 1990. Her research interests focus on materials for Li-ion batteries, Na-ion batteries, and solid-state batteries.

Wei Yin received her M.S. in Materials Science from Huazhong University of Science and Technology in 2015 and her Ph.D. in Physics and Chemistry of Materials from Sorbonne University in 2019. She worked as a Postdoctoral Fellow in the Energy Storage and Distributed Resources Division at Lawrence Berkeley National Laboratory (LBNL) under supervision of Dr. Marca Doeff during 2020−2023. She is currently a battery engineer at Joby Aviation. Her research interests focus on fundamental redox chemistry and materials development for batteries.

Juhyeon Ahn is a project scientist of the Energy Storage and Distributed Resources Division at LBNL, where she joined as a postdoctoral fellow in 2019. She was also a postdoctoral researcher at Korea Institute of Science and Technology (KIST). She received her B.E. and M.S. in Environmental Biological Engineering from Myongji University, and her Ph.D. in Chemical Engineering from Yonsei University. Previously, she worked as a visiting fellow at National Research Council Canada (NRC). Her research interests include discovery of new materials and knowledge through advanced characterization for energy storage and batteries applications.

Gözde Barim received her B.S. and M.S. in Chemistry from Bilkent University, Ankara, Turkey, in 2011 and 2013, respectively, and her Ph.D. in Chemistry from the University of Southern California in 2018. She joined the Lawrence Berkeley National Laboratory in 2019 and worked as a postdoctoral fellow under the supervision of Dr. Marca Doeff in the Energy Storage and Distributed Resources Division before joining Cuberg in 2022. Her research interests focus on the development of materials for energy storage devices including Li-ion batteries, Na-ion batteries, and Li-metal batteries.

Judith Alvarado received her PhD from UC San Diego in Materials Science and Engineering where she focused on the characterization of the solid electrolyte interphase for both lithium and sodium ion batteries. She completed a postdoctoral fellowship at Lawrence Berkeley National Laboratory in the Energy Storage and Distributed Resources Division. Judith now works in industry where she is focused on making a direct impact to combat climate change.

Authors (left): from left to right Dr. Gozde Barim, Dr. Marca Doeff, Dr. Judith Alvarado, and Dr. Wei Yin. (right) Dr. Juhyeon Ahn.

Introduction

In intercalation systems, alkali metal cations shuttle between two host structures that undergo insertion processes at different potentials. This forms the basis not only of technologically important Li-ion batteries (LIBs) but also emerging sodium-ion batteries (NIBs),[1-3] which are gaining attention due to sustainability arguments.[4] In principle, the cells that comprise these devices are very similar (**Figure 1**) consisting of composite cathodes and anodes on metallic current collectors, separated by membranes wetted by ionically conductive electrolytic solutions, although the exact materials differ.

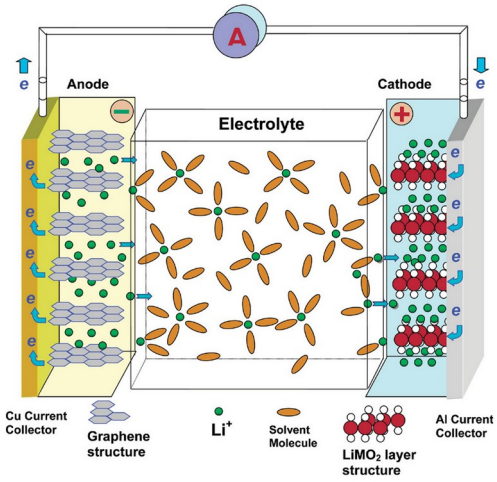

Figure 1. Schematic of a cell in a Li-ion battery. A cathode (positive electrode) supported by a current collector (on the right) is separated from the anode (negative electrode) on a current collector (on the left) by a porous membrane, which allows ions, but not electrons, to travel from one electrode to another. Electrons travel through an external circuit as the cell is operating. The set-up for Na-ion batteries is similar, with Na^+ ions replacing Li^+ ones. Reproduced with permission from reference [5]. Copyright 2004 American Chemical Society.

Layered transition metal oxides or polyanionic compounds are generally used as cathode materials in both Li-ion and Na-ion configurations, although there is a greater array of choices

for the latter than for the former. In LIBs, anode materials are commonly based on graphite, either used alone or as a blend with small amounts of silicon, which alloys with lithium at low potentials. While lithium can insert into graphite up to a composition of LiC_6 (corresponding to a theoretical capacity of ~370 mAh/g), sodium inserts only to a composition of NaC_{64}. The difference is not due to size (consider that potassium can form a graphite intercalation compound with composition KC_8) rather it is due to a lattice mismatch.[6] Instead, hard carbons are often used as anode materials for Na-ion batteries.[7] Optimized materials can have capacities exceeding 300 mAh/g and undergo redox through a combination of processes including sodium intercalation between graphene layers in the small, ordered domains, chemisorption in defects, and insertion into micropores and nanopores. The densities of hard carbons range from 1.4−1.8 g/cc, lower than that of graphite at 2.26 g/cc. Low density has an adverse effect on energy density, all other things being equal. There are also safety concerns associated with low potentials at which some carbons insert sodium because of the risk of plating.[8] Finally, the state of hard carbon commercialization is still in early stages and most production is currently in China, raising supply security concerns.[9] For these reasons, investigation into alternatives to hard carbons is warranted.

Some promising alternatives, based on wide availability, higher densities (~2.5−3.5 g/cc), low toxicities, and low precursor costs, are titanates. Sodium insertion into nanostructured anatase[10] or rutile[11] forms of binary titanates occurs at fairly high average potentials (~0.8V vs. Na^+/Na). However, a ternary stepped layered titanate, $Na_2Ti_3O_7$,[12] is electrochemically active at a much lower potential of about 0.3V vs. Na^+/Na, making it more suitable as an anode, although its long-term reversibility is not clear. The poor cycling and rate behavior have been attributed to side reactions, instability of the SEI, and a transition to a poorly electronically conductive phase

at the top of charge.[13] Strategies to improve performance include optimization of synthesis and electrode fabrication, reduction of particle size, and the use of carbon coatings and reduced graphene oxide to improve electronic conductivity. These have met with some success, although practical capacities (~180 mAh/g) are still lower than the theoretical predicted value of 311 mAh/g. We have recently investigated two other classes of titanate materials that have favorable properties, including high capacities and low average insertion potentials, for use as anodes in sodium-ion batteries. These both have stepped layered structures similar to that of $Na_2Ti_3O_7$ as shown in **Figure 2**. The first is so-called "sodium nonatitanate" or NNT (**Figure 2a**),[14, 15] which has been used as an ion-exchanger for nuclear waste clean-up,[16] and which has a composition of $Na_2Ti_3O_6{\cdot}2H_2O$[17] prior to thermal treatment.

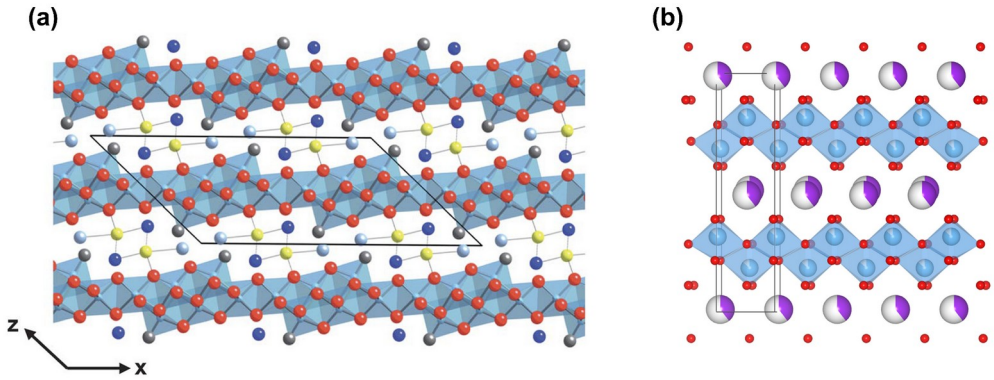

Figure 2. a) Structure of as-made "sodium nonatitanate (NNT)". $Ti^{4+}O_6$ octahedra (in blue) are linked together into steps six units across. Sodium ions and water molecules (yellow and blue spheres, respectively) are located between the stepped layers. Reprinted with permission from reference 14. Copyright 2013 Royal Society of Chemistry. **b)** Lepidocrocite-type titanate structure. $Ti^{4+}O_6$ octahedra (in blue) are linked together into corrugated layers, between which large exchangeable cations (purple/white spheres) and, sometimes, water molecules are located.

A second class of titanate materials is structurally related to the iron-containing mineral lepidocrocite, having corrugated layers (or steps one $Ti^{4+}O_6$ unit across) as shown in **Figure 2b**.[19-21] The general formula for the as-made materials is $A_xTi_{2-y}M_yO_4$ where A is a large monovalent cation, which is readily exchanged, and M stands for a wide variety of substituents such as Li^+ or Mg^{2+} or a vacancy (designated by $\ominus$ hereafter). The values of x and y are correlated so that Ti is always in the tetravalent state, and solid solution behavior is often exhibited. The positions of interlayer species and the orientation of the titanate layers with respect to one another vary with the chemistry, so that several space groups are possible.

Our early work on NNT and the sodium-exchanged version of $K_{0.8}Ti_{1.73}Li_{0.27}O_4$[22] showed that these materials inserted sodium reversibly at low average potentials (0.3−0.5V vs. Na^+/Na) making them good candidates as anode materials for NIBs. However, performance was far from optimum, prompting us to carry out further work designed both to understand the limitations and to improve the electrochemistry. What follows is a summary of the work carried out to date. Optimized half-cells containing the best materials can now deliver more than 200 mAh/g for hundreds of cycles at moderate current densities and can be utilized as anodes in full cells with suitable cathode materials, as described below.

Improvements to Sodium Nonatitanate (NNT) Electrochemistry

As-made NNT contains water, which is known to have an adverse effect on cell performance. Sodium half-cells containing NNT that has not been heat-treated to remove water show high first cycle coulombic inefficiencies and very poor reversibility, particularly when polyvinylidene fluoride (PVdF) is used as the binder in the composite electrode.[14] Results are somewhat improved when PVdF is replaced with a more compliant carboxymethylcellulose

(CMC) binder although first cycle C.E.s are still poor.[23] Unlike PVdF, CMC contains functional groups that interact strongly with active materials preventing cracking or disconnection that can lead to capacity loss during cycling. It has been used to improve electrochemical performance of cells containing electrodes that undergo large volume changes during cycling, such as silicon.[24, 25] Because of the larger size of the sodium ion compared to lithium, volume changes are more severe in sodium systems and cycling is generally better when CMC is used compared to PVdF. Still, the low potential at which NNT inserts results in irreversible side reactions involving electrolytic solution and binder and formation of a protective SEI layer during the first cycle on particle surfaces. Irreversible reduction of water to hydrogen at low potentials contributes to the inefficiency.

Water may be removed from NNT by heating in air or argon. The material is thermally stable up to between 600–700 °C, depending on rate of heating and atmosphere, before it decomposes to form the tunnel-containing $Na_2Ti_6O_{13}$, layered $Na_2Ti_3O_7$, and other phases.[14, 23] Heating to 600 °C results not only in removal of interlayer water, but a decrease in the *c*-axis of 12% and rearrangement of sodium ions to form O-Na-O bridges yielding a pseudo-tunnel structure (**Figure 3a**). This structure does not take up water between the titanate layers upon exposure to atmosphere. Water uptake between layers in the as-made material upon exposure to water or humid atmosphere can be readily observed in the XRD patterns by the shift of the strong low angle peak to larger d-spacings and/or its doubling,[23] indicative of two phases with different water contents. Gentle heating for a short period of time removes the second peak and induces a shift of this reflection back to the original value. In contrast, the XRD pattern of NNT heated to 600 °C does not change after it has been exposed to moist atmosphere. **Figure 3b**

shows the voltage profiles at the second cycles of cells containing NNTs heated to various temperatures, using a CMC binder for the electrode fabrication. The highest capacity of about 200 mAh/g is obtained for the cell containing NNT material heated to 500 °C. Good cycling can be obtained for this material when it is carbon-coated through a sucrose pyrolysis method, which ameliorates the low initial electronic conductivity. Graphene wrapping of NNT by adding 1 wt% graphene oxide (GO) to the hydrothermal reactor during synthesis achieves the same aim; **Figure 3c** shows voltage profiles as a function of cycle number for a cell containing this material heated to 500 °C. (Note that GO is reduced during the first cycle at low potentials). **Figure 3d** shows a comparison of NNT electrodes made different ways, with CMC (in blue) or PVdF (in red) binder. One set of data (in black) shows results for a cell containing a carbon-coated (carbon made from sucrose) NNT electrode made with CMC. This shows the clear positive effect of using CMC and carbon-coating on reversibility. The highest 1st cycle C.E. is found with the graphene-wrapped NNT in **Figure 3c**, however.

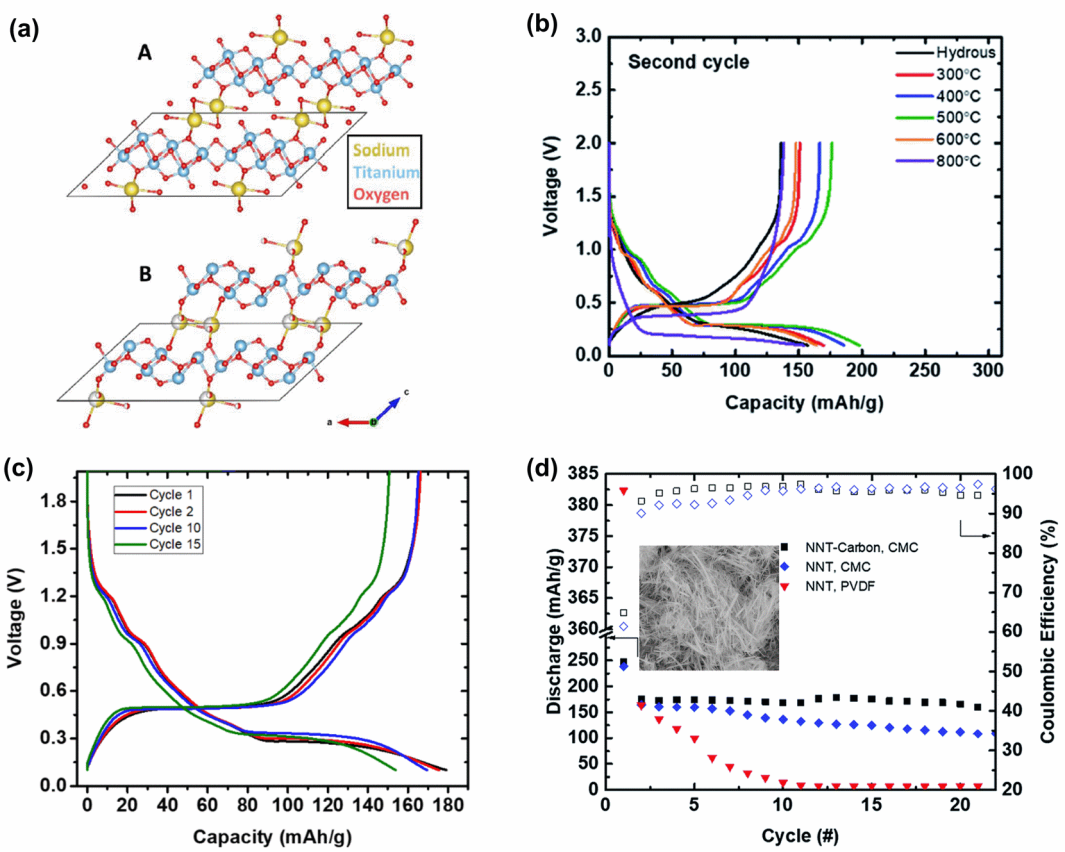

Figure 3. a) Structure of as-made NNT (A, top) and after heating to 600 °C (B, bottom). **b)** Voltage profile at second cycles of cells containing NNT heated to the indicated temperatures. **c)** Voltage profile with increasing cycle number of cells containing graphene-wrapped NNT heated to 500 °C and **d)** cycling performance for cells containing different types of NNT electrodes, inset shows Scanning Electron Microscopy (SEM) image of NNT. Reproduced with permission from reference [23]. Copyright 2020 Royal Society of Chemistry.

Lepidocrocite-type titanates

The sodium-exchanged version of KTL ($Na_{0.8}Ti_{1.73}Li_{0.27}O_4$), a lepidocrocite-type titanate showed promising electrochemical properties, but Mg-substituted variants such as $Na_{0.7}Ti_{1.45}Mg_{0.35}O_4$ or $Na_{0.9}Ti_{1.55}Mg_{0.45}O_4$ perform very poorly in sodium half-cells.[26] Density functional theory calculations described in reference 26 indicate that Li^+ ions in $Na_{0.8}Ti_{1.73}Li_{0.27}O_4$

can drop into the sodium layers, providing additional diffusional pathways, whereas Mg^{2+} is immobile in the Mg-containing compounds. This suggests strongly that vacancies in the titanate layers may be beneficial for the electrochemical performance of lepidocrocite-type titanates. To test this theory, a series of $Na_xTi_{2-x/4\ x/4}O_4$ ($0.74 \leq x \leq 1$) materials were prepared from the Cs-containing precursors and tested.[27] A comparison of the second discharges of sodium half-cells containing $Na_{0.74}Ti_{1.815\ 0.185}O_4$ (red) and $Na_{0.8}Ti_{1.73}Li_{0.27}O_4$ (blue) is shown in **Figure 4a**. The former shows significantly greater capacity than the latter, although this is in part due to the availability of more sites for sodium insertion. To show the effect of changing the sodium content on theoretical capacities on the series of $Na_xTi_{2-x/4\ x/4}O_4$ ($0.74 \leq x \leq 1$) materials, theoretical capacities considering titanium content and site availability are shown in **Figure 4b**. Lower values of x (less sodium) result in higher theoretical capacities no matter which criterion is used; nevertheless, all the materials deliver somewhat more than predicted based on the site limitation argument, although less than that predicted if titanium content were the only determining factor. Note also, that the material with x = 0.8 still has a significantly higher practical capacity than $Na_{0.8}Ti_{1.73}Li_{0.27}O_4$; 220 mAh/g rather than 150 mAh/g.

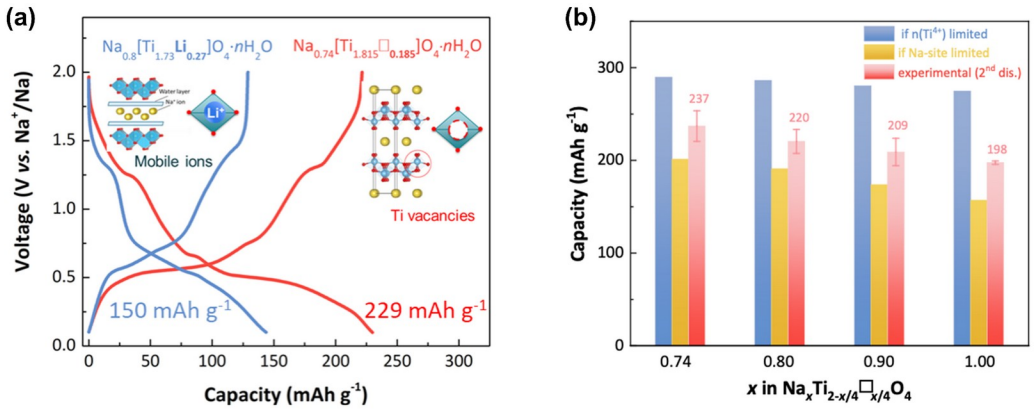

Figure 4. a) Voltage profiles of second cycles of sodium half-cells containing $Na_{0.74}Ti_{1.815\ 0.185}O_4$ (red) and $Na_{0.8}Ti_{1.73}Li_{0.27}O_4$ (blue). **b)** Theoretical capacities based on titanium content (blue bar) or site availability (yellow bar), and experimentally found capacities (red bar) for the $Na_xTi_{2-x/4\ x/4}O_4$ series. Reproduced with permission from reference [27]. Copyright 2021 Springer Nature.

The electrochemistry of the lepidocrocite-type titanates is also influenced by the identity of the interlayer cations. Cs ions in the parent material $Cs_{0.74}Ti_{1.815}\ominus_{0.185}O_4$ may be exchanged not only for Na^+, but also for other monovalent or divalent cations under mild conditions, as described in the Experimental section. **Figure S1a** shows XRD patterns for the original Cs-containing material, as well as for materials exchanged with Li^+, Na^+, K^+, Rb^+, or Mg^{2+}. In some cases (Li^+, K^+, and Mg^{2+}), patterns are complicated by the presence of hydrated phases, as evidenced by doubling of peaks. The positions of the (020) reflections at low angles also vary with the identity of the cation, indicating different interlayer spacings. TGA on the as-made materials (**Figure S1b**) shows that weight loss below about 200 ˚C, most likely due to removal of water, has an approximately inverse relationship to the size of the cations in the interlayer spaces. The material with the smallest cation, Li^+, which has the largest hydration radius,[28] contains the most water, whereas those with large cations like Rb^+, which have smaller hydration radii, have lower water contents. Raman spectra on the as-made materials (**Figure S1c**), show the same general features above the Raman shift value of 200 cm^{-1}, although red- or blue-shifted due to differences in bond-lengths induced by the different cations. Finally, Ti K-edge XAS data shows that Ti is tetravalent in all of the materials (**Figure S1d**). In summary, these data confirm that the layered structure of the parent $Cs_{0.74}Ti_{1.815}\ominus_{0.185}O_4$ is maintained for the ion-exchanged materials.

Figure S1e and **f** show 5th cycle voltage profiles and cycling performance for half-cells containing these materials after drying under vacuum at 100 ˚C. Capacities are lower for cells containing the materials with large cations (Rb^+ and K^+) than for $Na_{0.74}Ti_{1.815}\ominus_{0.185}O_4$ (shown in yellow). A similar effect has been observed when comparing $K_{0.8}Ti_{1.73}Li_{0.27}O_4$[29] and $Na_{0.8}Ti_{1.73}Li_{0.27}O_4$[22] electrodes performance and is attributable to the reduction in the number of available interlayer sites when larger cations are present and the relatively lower mobility of these cations, which may hamper diffusion of sodium ions. It is not clear at present why the Li^+-exchanged material (shown in green) also shows reduced capacity, although the smaller interlayer spacing of the material after drying may play a role. Interestingly, the capacities of cells containing $Mg_{0.37}Ti_{1.815}\ominus_{0.185}O_4$ are less compromised than those containing $Li_{0.74}Ti_{1.815}\ominus_{0.185}O_4$. During the exchange process, Mg^{2+} cations replace two monovalent cations, freeing some interlayer sites. The additional number of sites counteract the negative effects of low Mg^{2+} mobility and reduced interlayer spacing. Cells containing this material also seem to cycle somewhat better than those with $Na_{0.74}Ti_{1.815}\ominus_{0.185}O_4$ dried at 100 ˚C.

Effect of Binder and Electrolytic Solution on Electrochemistry of Lepidocrocite-type Titanates

As with NNT, the coulombic efficiencies on the first cycle for cells containing $Na_{0.74}Ti_{1.815\ 0.185}O_4$ are less than 100% because of side reactions occurring at low potentials that result in the formation of a protective SEI layer. The first cycle C.E. varies considerably with the type of electrolytic solution used, with the highest value found when 0.5 M sodium tetraphenyl borate ($NaBPh_4$) in diethylene glycol dimethyl ether (DEGDME) is used (**Figure 5a**). 1st cycle C.E. is also dependent on the history of exposure of the electrode to air (**Figure 5b**) and to the binder used (**Figure 5c**). A binder-free electrode, while not practical, has the highest C.E.,

followed by one made with CMC/SBR (styrene butadiene rubber). This suggests that binder decomposition contributes to 1st cycle coulombic inefficiencies. Note that the sodium-exchanged titanates derived from $Cs_xTi_{2-x/4\ x/4}O_4$ contain water, although this can be removed easily by drying at temperatures as low as 60 °C under vacuum. Unlike heat-treated NNT, the materials dried at low temperatures are very hygroscopic and rapidly take up water upon exposure to atmosphere.

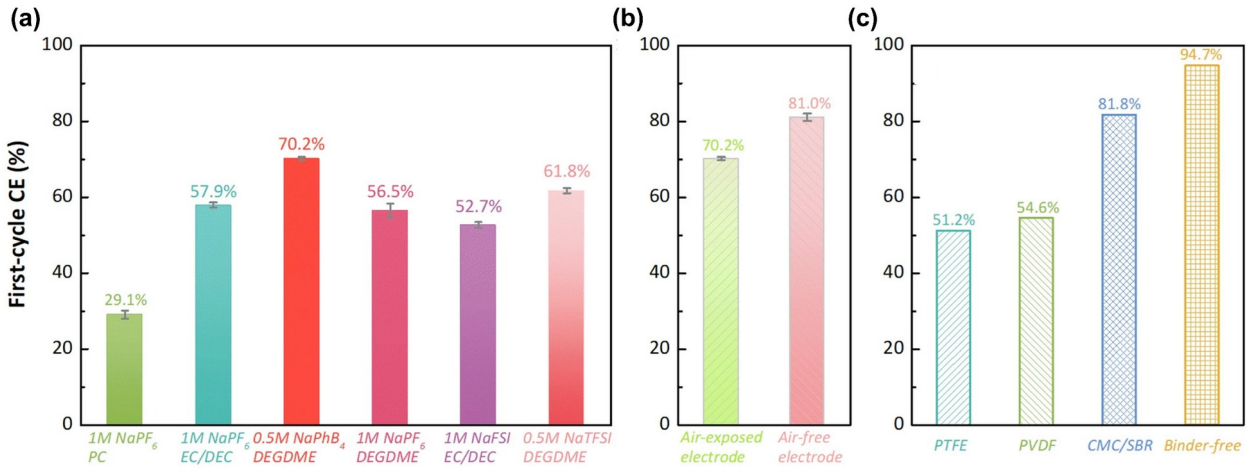

Figure 5. First cycle coulombic efficiencies in sodium half-cells containing $Na_{0.74}Ti_{1.815\ 0.185}O_4$ for **a)** the indicated electrolytic solutions, **b)** history of electrode air exposure, and **c)** binder used in the composite electrode. Reproduced with permission from reference [27]. Copyright 2021 Springer Nature.

Surface properties of lepidocrocite-type titanates: air exposure and thermal history

The fact that C.E. is influenced by the history of electrode exposure to air has some bearing on the observation that practical capacities exceed the theoretical values based on site limitation arguments in this system. A close look at the voltage curves of sodium half-cells containing air-exposed and air-excluded electrodes shows subtle differences during cycling

(**Figure 6a** and **b,** respectively). For example, the small plateau above 1V is much more distinct for the cell containing the air-excluded electrode. Power law analyses (Equation 1) of cyclic voltammetry data from sodium half-cells, which relates current (i) and scan rate (v), give information on the redox mechanism.

(1) $$i=av^b$$

A value of b close to 0.5 is typically found for diffusional processes, whereas b is 1 for surface-controlled reactions. The processes at around 0.5V, marked R2 and R2' for the air-excluded and air-exposed electrodes, as shown in **Figure 6c** and **d,** respectively, have b values of 0.67 and 0.69, indicating that they are primarily diffusional in nature. In contrast, R1, located at 1.25V, has a b value of 0.76 and R1' is 0.92, indicating a much higher contribution from surface-related processes. Surface functional groups, the nature of which depend on the history of air exposure, may provide additional redox-active sites. Minor changes observed in the Ti L-edge X-ray absorption spectrum (soft XAS, not shown) of the air-exposed electrode compared to that of the air-excluded one suggest that Ti is slightly reduced on the surface. This may occur due to hydroxylation of defect sites on particle surfaces during the brief exposure to moisture-containing atmosphere.

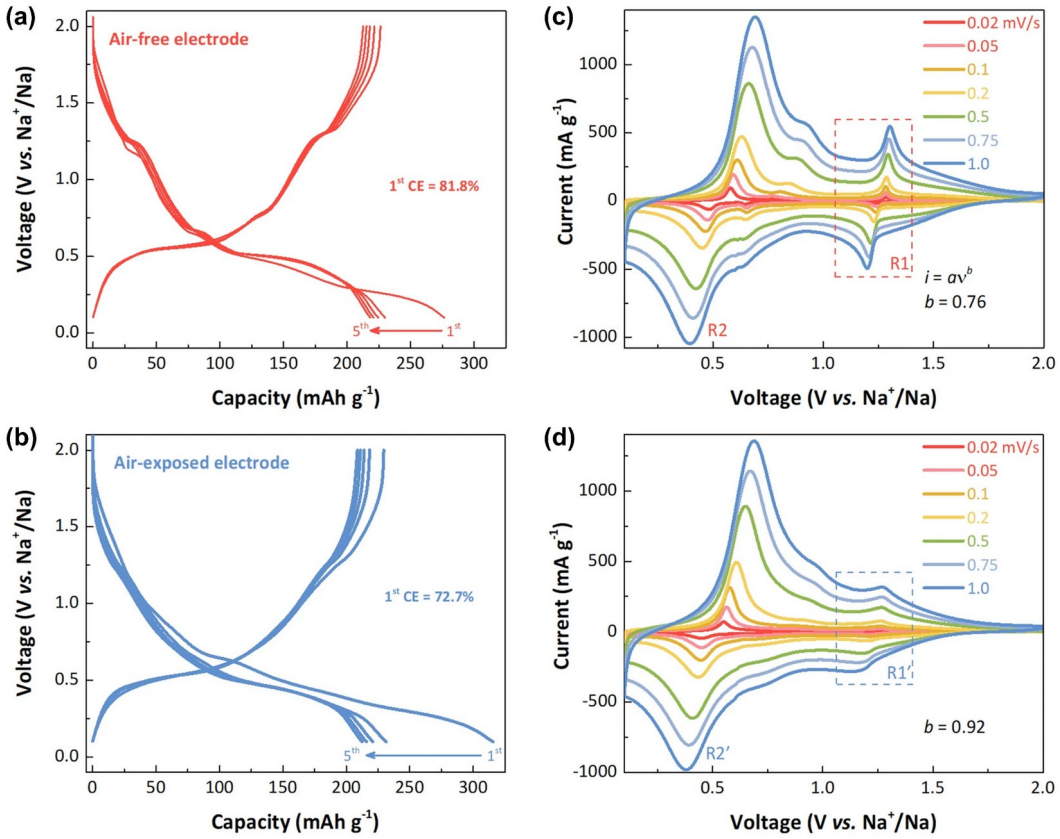

Figure 6. a,b) Voltage profiles for initial 5 cycles of sodium half-cells containing $Na_{0.74}Ti_{1.815}$ $_{0.185}O_4$ electrodes that (**a**) have not been exposed to air, and (**b**) have been exposed to air for 10 minutes. **c,d**) Cyclic voltammograms of cells containing (**c**) air-free and (**d**) air-exposed electrodes. Electrodes were made with CMC/SBR binder and 0.5 M $NaBPh_4$ in DEGDME was used as the electrolyte. Reproduced with permission from reference [27]. Copyright 2021 Springer Nature.

While the 1st cycle C.E. of the cells containing air-exposed electrode is less than that of those containing the air-excluded ones, the cycling is actually slightly better. An examination of the data reveals that capacity loss above 1V is mainly responsible for the fading in both types of cells, but that it is worse for the one with the air-excluded electrode than for the air-exposed one. This is further evidence for different surface chemistries depending on the history of air

exposure. To modify the surface properties, heating experiments on $Na_{0.74}Ti_{1.815\ 0.185}O_4$ were carried out.[30] As the temperature is raised, the material undergoes a series of transformations (**Figure 7a** and **b**). The initial structure (space group *Immm*) is maintained to about 150 °C, with shrinkage in the *b*-lattice parameter consistent with loss of interlayer water. In the anhydrous material, there is a rearrangement of Na^+ ions in the interlayer space from the original rectangular prismatic coordination (space group *Immm*, **Figure 7c**) to trigonal prismatic (space group *Cmcm*, **Figure 7d**). Similar to NNT, the material decomposes above 700 °C to form the tunnel compound $Na_2Ti_6O_{13}$ and other phases, with unknown structures forming at intermediate temperatures.

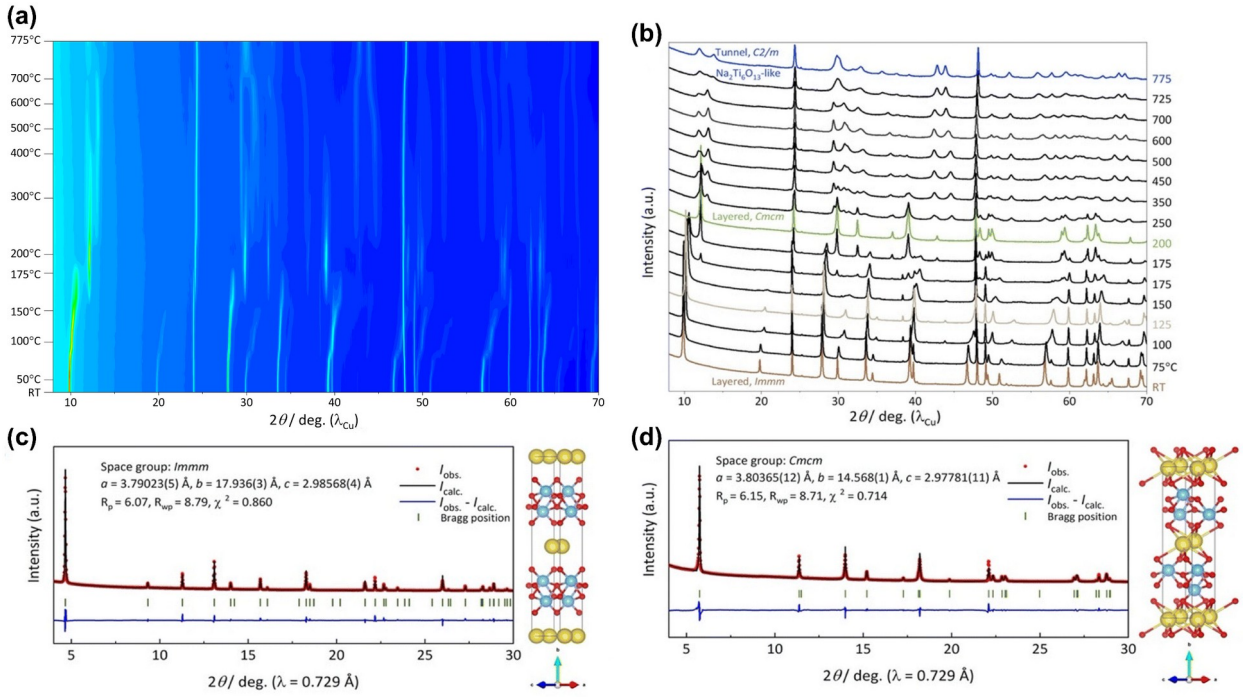

Figure 7. a) *In situ* thermal synchrotron XRD patterns collected on $Na_{0.74}Ti_{1.815}\ominus_{0.185}O_4$ (two-dimensional contour plot, and **b**) selected profiles as a function of temperature. **c,d)** Fitted patterns of **(c)** low temperature *Immm* structure and **(d)** intermediate temperature *Cmcm*

structure. Reproduced with permission from reference [30]. Copyright 2022 Royal Society of Chemistry.

The electrochemical properties of $Na_{0.74}Ti_{1.815\ 0.185}O_4$ heated to various temperatures are shown in **Figure 8**. The capacity of the half-cell containing the material heated to 500 °C gradually increases with cycle number when a lower cut-off voltage limit of 0.1V is used throughout the cycling (**Figure 8a**). If this limit is lowered to 0.05V only on the first cycle, the higher capacity is realized on subsequent cycles even if the lower cut-off voltage is increased to 0.1V (**Figure 8b**). *Ex situ* XRD experiments and high-resolution TEM on partially and fully discharged electrodes show that this material gradually becomes amorphous as sodium is inserted on the first cycle and that this process is irreversible.[26]

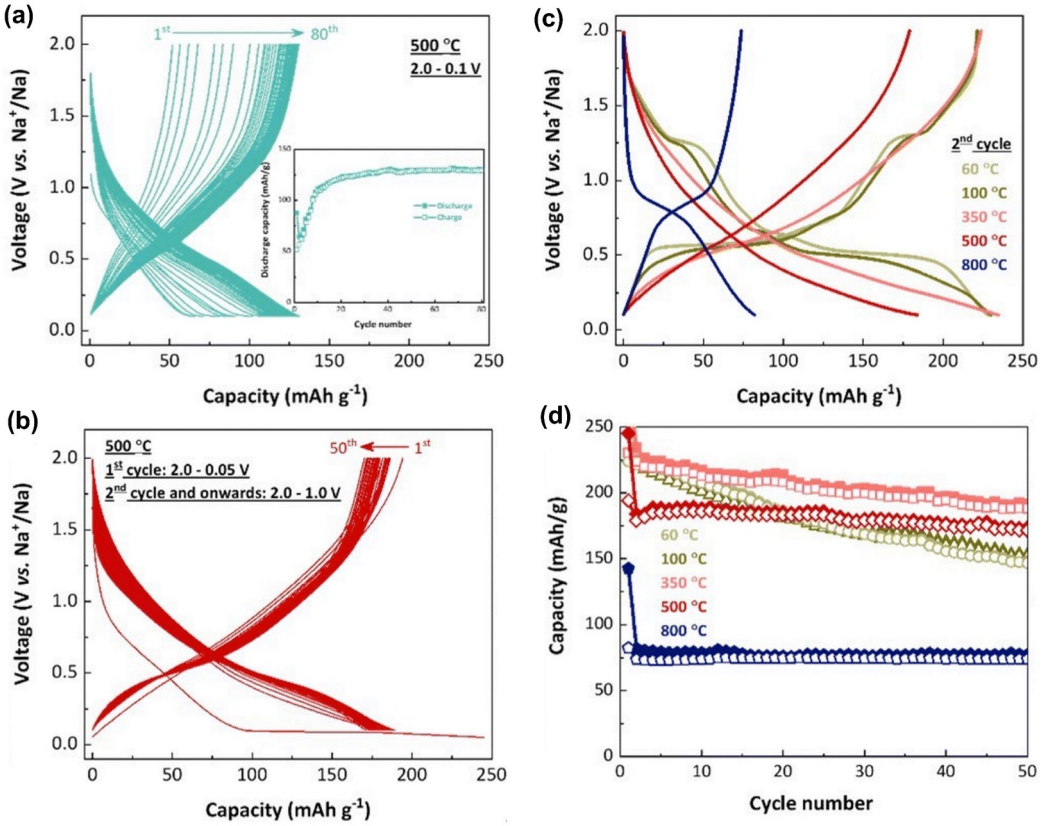

Figure 8. a,b) Voltage profiles during cycling of half-cells containing $Na_{0.74}Ti_{1.815}\ominus_{0.185}O_4$ heated to 500 °C within the voltage ranges over **(a)** 2.0–0.1V and **(b)** 2.0–0.05V on cycle 1 and 2.0–0.1V thereafter; **c,d)** Comparisons of **(c)** voltage profiles at second cycles of cells containing $Na_{0.74}Ti_{1.815\ 0.185}O_4$ heated to the indicated temperatures and **(d)** cycling performance. All cells contained 0.5 M $NaBPh_4$ in DEGDME as the electrolyte. Reproduced with permission from reference [30]. Copyright 2022 Royal Society of Chemistry.

The voltage profiles at second cycles of cells containing $Na_{0.74}Ti_{1.815\ 0.185}O_4$ heated to various temperatures is shown in **Figure 8c**. It is clear that the processing temperature has a profound effect on the electrochemistry. Most of the cells with materials heated to temperatures above 100 °C exhibit sloping voltage profiles with no feature near 1.25V. The only exception is the one with the material heated to 800 °C, which shows a plateau near 0.9V, similar to what is found for $Na_2Ti_6O_{13}$.[31, 32] Capacity retention is markedly improved for the cells containing electrode materials heated to 500 °C (**Figure 8d**). Most notably, there is less fading in the high voltage region compared to that of cells containing $Na_{0.74}Ti_{1.815\ 0.185}O_4$ heated to 60 °C. There appears to be less capacitive (surface) contribution to the electrochemistry in the case of $Na_{0.74}Ti_{1.815\ 0.185}O_4$ heated to 500 °C than for the material heated to 60 °C based on this observation. However, an analysis of Ti K-edge XAS data on pristine and discharged electrodes indicates that less titanium is reduced than expected for a pure reductive intercalation mechanism, suggesting a hybrid process for both types of materials.[26] Thus, changes induced by heating involve not only transformation of the bulk structure but that of the surface chemistry as well.

The surface chemistry can also be modified simply by a carbon coating process. Since 60 °C-heated $Na_{0.74}Ti_{1.815}\ominus_{0.185}O_4$ undergoes structural change above 150 °C, the material was carbon-

coated at low temperatures by grinding with soft carbon (acetylene black) to preserve its initial layered structure. The color-change and morphology of the powders are shown in **Figure S2a** and **b**. The plateau at 1.25V disappears in cells containing the carbon-coated material (**Figure S2c**), and while capacity is initially lower, the cycling is greatly improved (**Figure S2d**). This provides additional evidence for the influence of surface properties on the redox chemistry of $Na_{0.74}Ti_{1.815\ 0.185}O_4$. The addition of carbon nanotubes further improves capacity without compromising cycling behavior.

Full-cell cycling

Cycling in full cells was attempted using $Na_{0.74}Ti_{1.815\ 0.185}O_4$ dried at 60 ˚C as the anode and $Na_3V_2(PO_4)_3$ (NVP) as the cathode. **Figure S3** shows a half-cell with NVP as the cathode using 0.5 M $NaPhB_4$ in DEGDME as the electrolyte. The cell delivers 112 mAh/g (**Figure S3a**), close to the theoretical value based on NVP.[33] Because this electrolyte is not expected to have good oxidative stability over the long term, 1 M $NaPF_6$ in EC/DEC was substituted in the full cells (**Figures S3b** and **c**). Some coulombic inefficiency is observed on the first cycle (**Figure S3b**) in cells where the negative/positive (N/P) ratio is close to 1, because of losses due to SEI formation on the anode side. (Note that in this configuration, the cell is charged initially, meaning that sodium ions are extracted from the NVP cathode and inserted into $Na_{0.74}Ti_{1.815\ 0.185}O_4$). This led to a lower capacity than expected based on the NVP cathode. Using a pre-cycled anode in the full cell improved the results, and led to nearly full utilization of the cathode (**Figure S3c**). These results show that $Na_{0.74}Ti_{1.815\ 0.185}O_4$ can be successfully used as an anode in full cells. However, the low electronic conductivity of the pristine titanate materials is

likely to limit performance in batteries with unconventional configurations such as extremely thick electrodes or flow batteries using slurries.

Heterostructures

To overcome the low electronic conductivity, we prepared two types of heterostructures, in which carbon is interleaved with the titanate layers.[18, 34] Heterostructuring has also been used recently to prepare cathode materials for sodium-ion batteries.[35] The first step, in both cases, was to exfoliate $K_{0.8}Ti_{1.73}Li_{0.27}O_4$ to produce titania nanosheets (**Figure 9a**) using previously described literature procedures.[36, 37] The nanosheets were then combined with either dopamine hydrochloride or reduced graphene oxide (rGO) to form self-assembled heterostructures. In the first case, an additional calcination step was used to transform the dopamine into carbon. By varying synthesis conditions and precursor ratios, the carbon content in the heterostructures could be tuned to between 17.5−30% (carbonized dopamine samples) or 1−17% (graphene samples). XRD patterns of both types of materials show broadened peaks with the low-angle (020) reflections shifted to larger d-spacings, with the degree of shift roughly proportional to the amount of carbon in the heterostructures. High-resolution transmission electron microscopy (HRTEM) of the heterostructure containing 8.5% rGO (**Figure 9b−d**) show that the material is heterogeneous, with a range of d-spacings, some of which correspond to graphene (0.35 nm) or titania nanosheets (0.8 nm) as well as expanded layers (1.1 nm). This suggests that there was partial re-stacking of titania and graphene during the synthesis process. In contrast, bright field transmission electron microscopy (BFTEM) and high angle annular dark field-scanning transmission electron microscopy (HAADF-STEM) images show more comprehensive

interleaving for a heterostructure containing 30% carbon made from dopamine, which has a repeating layer spacing of ~1.3 nm (**Figure 9e** and **g**).

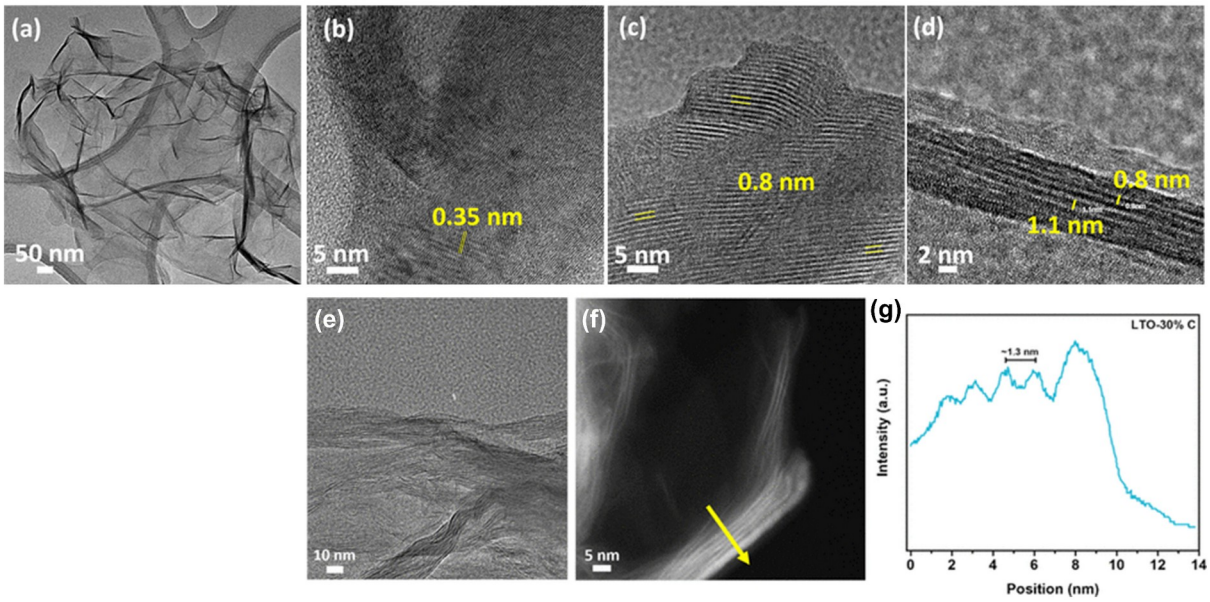

Figure 9. a) TEM of titania nanosheet. **b–d)** HRTEM images of heterostructured titanate-8.5% rGO. Reprinted with permission from references [18]. Copyright 2022 American Chemical Society. **e)** BFTEM, **f)** HAADF-STEM images, and **g)** average line histogram extracted by analyzing the region outlined by the yellow arrow in (**f**) of heterostructured titanate-30%C made from dopamine. Reprinted with permission from references [34]. Copyright 2021 American Chemical Society.

Coagulated titania nanosheets with no carbon between the layers are somewhat electroactive, although the capacities are less than 100 mAh/g in sodium half-cells, even when acetylene black is added to the electrodes to counteract the low electronic conductivity. To investigate the properties of the heterostructures, composite electrodes were fabricated without adding carbon conductor (e.g. acetylene black) beyond what was already in the active materials.

Sodium half cells containing these electrodes exhibited featureless sloping voltage profiles with average potentials about 0.6V vs. Na^+/Na. The capacities of half-cells increased with carbon content in the dopamine-derived carbon heterostructures, reaching a maximum of about 200 mAh/g on the second cycle for the 30%C sample.[34] Lower capacities were obtained for cells with the graphene-containing heterostructures, with the maximum of about 120 mAh/g achieved for the 8.5% graphene sample.[18] Heterostructures with higher graphene contents than this actually performed worse, probably reflecting the negative effects of graphene re-stacking on electrochemical performance (Electrodes consisting of pure rGO are electrochemically inert).

Impedance analyses on cells containing composite electrodes with titania nanosheets and added acetylene black showed a several orders of magnitude increase in resistance at the top of charge, attributable to increased charge transfer resistance on the positive side. In contrast, the charge transfer resistance was greatly reduced for the cells containing heterostructured materials even in the absence of added acetylene black in the composite electrodes. The reduced charge transfer resistance tracked carbon content in the heterostructures, with the best results observed for cells containing the titania-30% carbon derived from dopamine electrodes. Thus, heterostructuring proves to be much more effective at reducing charge transfer resistance than simply adding carbon to the composite electrode.

Insertion of sodium ions into heterostructured titania-23.4%C made from dopamine induced an irreversible change in symmetry, as evidenced in *ex situ* synchrotron XRD experiments by a near doubling of the low angle *d*-spacing compared to the pristine material. This is reminiscent of the phase change seen during ion-exchange of $K_{0.8}Ti_{1.73}Li_{0.27}O_4$ (space group *Cmcm*) with sodium.[22] In that case, the space group changes to *Pmmm*, with a shift of the titanate layers by *a*/2 and a change in cation coordination from trigonal prismatic to cubic. Ti K-

edge XAS results on similar electrodes show that Ti is partially reduced upon insertion of sodium, confirming the reductive intercalation (diffusional) mechanism. However, quantitative analyses of the spectra show that less titanium is reduced than expected based on the coulometry.

Although surface processes could account for this, another likely explanation is that insertion of sodium ions into interlayer carbon adds to the capacity.

These examples show how the electrochemical properties of stepped layered titanates can be tuned through changing synthesis and processing parameters. Other important factors for ensuring good reversibility and minimizing first cycle coulombic inefficiencies include careful consideration of binder and electrolytic solutions. Optimized materials can deliver 200 mAh/g or more in sodium half-cell configurations reversibly, with average potentials ranging from 0.3–0.6V vs. Na^+/Na. These make them suitable for use as anodes in sodium-ion batteries. Another consideration is the cost of processing. In this regard, NNT may be a more practical material than the lepidocrocite-type titanates, because of the simpler synthesis method, which does not require ion-exchange.

Conclusions

Two classes of stepped layered titanates, sodium nonatitanate (NNT) and lepidocrocite-type titanates, have been presented as potential anode materials for sodium ion batteries. Both types undergo reversible reductive intercalation of sodium ions at low potentials, making them suitable for this application. The reversibility and first cycle coulombic efficiencies are sensitive to the binder used in the composite electrodes as well as the type of electrolyte used in cells. Some of the lepidocrocite titanates exhibit a hybrid redox mechanism involving surface reactions (pseudocapacitance) at potentials above 1V vs. Na^+/Na, which differ depending on the history of air exposure. The pseudocapacitance is primarily responsible for the capacity fading that is

observed. Modification of materials either by carbon coating or thermal treatment changes the surface properties and improves cycling stability of the cells. The lepidocrocite-type titanates can also be ion-exchanged with various monovalent or divalent cations, leading to different electrochemical properties. Finally, it is possible to incorporate carbon as a guest species in the interlayer space, leading to novel heterostructured materials that appear to have improved electronic conductivity.

Supporting Information: experimental details for unpublished results, XRD patterns, TGA results, Ti K-edge data, half-cell data for ion-exchanged lepidocrocite-type titanates, SEM images and half-cell data for carbon-coated lepidocrocite-type titanates, full cell data for lepidocrocite-type titanates with NVP cathode.

Acknowledgments

This work was supported by the Assistant Secretary for Energy, Efficiency and Renewable Energy, Office of Vehicle Technologies of the U.S. Department of Energy under Contract No. DE-AC02-05CH11231. The heterostructure work was supported as part of the Center for Mesoscale Transport Properties, an Energy Frontier Research Center supported by the U.S. Department of Energy, Office of Science, Basic Energy Sciences, under award#DE-SC0012673 including the following. Work at the Molecular Foundry of Lawrence Berkeley National Lab (LBNL), supported

by the Office of Science, Office of Basic Energy Sciences of the U.S. Department of Energy under Contract No. DE-AC02-05CH11231. We would like to acknowledge the use of the Stanford Synchrotron Radiation Lightsource, SLAC National Accelerator Laboratory, that is

supported by the U.S. Department of Energy, Office of Science, Office of Basic Energy Sciences under Contract No. DE-AC02-76SF00515.

References

1. Rudola, A.; Sayers, R.; Wright, C. J.; Barker, J., Opportunities for moderate-range electric vehicles using sustainable sodium-ion batteries. *Nat. Energy* **2023**, *8* (3), 215-218.

2. Rudola, A.; Rennie, A. J. R.; Heap, R.; Meysami, S. S.; Lowbridge, A.; Mazzali, F.; Sayers, R.; Wright, C. J.; Barker, J., Commercialisation of high energy density sodium-ion batteries: Faradion's journey and outlook. *J. Mater. Chem. A* **2021**, *9* (13), 8279-8302.

3. Abraham, K. M., How Comparable Are Sodium-Ion Batteries to Lithium-Ion Counterparts? *ACS Energy Lett.* **2020**, *5* (11), 3544-3547.

4. Vaalma, C. B. D., Weil, M. and Passerini, S., A cost and resource analysis of sodium-ion batteries. *Nat. Rev. Mater.* **2018**, *3*, 1-11.

5. Xu, K., Nonaqueous Liquid Electrolytes for Lithium-Based Rechargeable Batteries. *Chem. Rev.* **2004**, *104*, 4303-4417.

6. Dresselhaus, M. S. D., G., Intercalation Compounds of Graphite. *Adv. Phys.* **2002**, *51* (1), 1-186.

7. Dou, X.; Hasa, I.; Saurel, D.; Vaalma, C.; Wu, L.; Buchholz, D.; Bresser, D.; Komaba, S.; Passerini, S., Hard carbons for sodium-ion batteries: Structure, analysis, sustainability, and electrochemistry. *Mater. Today* **2019**, *23*, 87-104.

8. Chen, D.; Zhang, W.; Luo, K.; Song, Y.; Zhong, Y.; Liu, Y.; Wang, G.; Zhong, B.; Wu, Z.; Guo, X., Hard carbon for sodium storage: mechanism and optimization strategies toward commercialization. *Energy & Environ. Sci.* **2021**, *14* (4), 2244-2262.

9. Liu, H.; Baumann, M.; Dou, X.; Klemens, J.; Schneider, L.; Wurba, A.-K.; Häringer, M.; Scharfer, P.; Ehrenberg, H.; Schabel, W.; Fleischer, J.; von der Aßen, N.; Weil, M., Tracing the technology development and trends of hard carbon anode materials - A market and patent analysis. *J. Energy Storage* **2022**, *56*, 105964.

10. Li, W.; Fukunishi, M.; Morgan, B. J.; Borkiewicz, O. J.; Chapman, K. W.; Pralong, V.; Maignan, A.; Lebedev, O. I.; Ma, J.; Groult, H.; Komaba, S.; Dambournet, D., A Reversible Phase Transition for Sodium Insertion in Anatase TiO_2. *Chem. Mater.* **2017**, *29* (4), 1836-1844.

11. Usui, H.; Domi, Y.; Sakaguchi, H., Rutile TiO_2 Creates Advanced Na-Storage Materials. *ACS Appl. Energy Mater.* **2023**, *6* (8), 4089-4102.

12. Senguttuvan, P.; Rousse, G.; Seznec, V.; Tarascon, J.-M.; Palacín, M. R., $Na_2Ti_3O_7$: Lowest Voltage Ever Reported Oxide Insertion Electrode for Sodium Ion Batteries. *Chem. Mater.* **2011**, *23* (18), 4109-4111.

13. Dong, J.; Jiang, Y.; Wang, R.; Wei, Q.; An, Q.; Zhang, X., Review and prospects on the low-voltage $Na_2Ti_3O_7$ anode materials for sodium-ion batteries. *J. Energy Chem.* **2024**, *88*, 446-460.

14. Shirpour, M.; Cabana, J.; Doeff, M., New materials based on a layered sodium titanate for dual electrochemical Na and Li intercalation systems. *Energy & Environ. Sci.* **2013**, *6* (8), 2538-2547.

15. Lehto, J.; Harjula, R.; Girard, A.-M., The equilibrium of strontium ion exchange on sodium titanate, $Na_4Ti_9O_{20}\cdot xH_2O$. *J. Chem. Soc., Dalton Trans.* **1989**, 101-103.

16. Yates, S. F.; Sylvester, P., Sodium Nonatitanate: A Highly Selective Inorganic Ion Exchanger for Strontium. *Sep. Sci. .Tech.* **2001**, *36* (5-6), 867-883.

17. Andrusenko, I.; Mugnaioli, E.; Gorelik, T. E.; Koll, D.; Panthofer, M.; Tremel, W.; Kolb, U., Structure analysis of titanate nanorods by automated electron diffraction tomography. *Acta crystallogra. B,* **2011**, *67* (Pt 3), 218-25.

18. Barim, G.; Yin, W.; Lin, J.; Song, C.; Kuykendall, T. R.; Takeuchi, K. J.; Takeuchi, E. S.; Marschilok, A. C.; Doeff, M. M., Lepidocrocite Titanate–Graphene Composites for Sodium-Ion Batteries. *J. Phys. Chem. C* **2022**, *126* (45), 19065-19073.

19. Gao, T.; Fjellvåg, H.; Norby, P., Protonic titanate derived from $Cs_xTi_{2-x/2}Mg_{x/2}O_4$ (x = 0.7) with lepidocrocite-type layered structure. *J. Mater. Chem.* **2009**, *19* (6), 787-794.

20. Groult, D. M., C; and Raveau, B., Nouveaux oxydes a structure en feuillets: Les titanates de potassium non-stoechiometriques $K_x(M_yTi_{2-y})O_4$. *J. Solid State Chem.* **1980**, *32*, 289-296.

21. Reid, A. F.; Mumme, W. G.; Wadsley, A. D., A new class of compound $M_xA_xTi_{2-x}O_4$ ($0.60 < x < 0.80$) Typified by $Rb_xMn_xTi_{2-x}O_4$. *Acta Crystallogr. B* **1968**, *24* (9), 1228-1233.

22. Shirpour, M.; Cabana, J.; Doeff, M., Lepidocrocite-type Layered Titanate Structures: New Lithium and Sodium Ion Intercalation Anode Materials. *Chem. Mater* **2014**, *26* (8), 2502-2512.

23. Alvarado, J.; Barim, G.; Quilty, C. D.; Yi, E.; Takeuchi, K. J.; Takeuchi, E. S.; Marschilok, A. C.; Doeff, M. M., Optimization of nonatitanate electrodes for sodium-ion batteries. *J. Mater. Chem. A* **2020**, *8* (38), 19917-19926.

24. Shobukawa, H.; Alvarado, J.; Yang, Y.; Meng, Y. S., Electrochemical performance and interfacial investigation on Si composite anode for lithium ion batteries in full cell. *J. Power Sources* **2017**, *359*, 173-181.

25. Nguyen, C. C.; Yoon, T.; Seo, D. M.; Guduru, P.; Lucht, B. L., Systematic Investigation of Binders for Silicon Anodes: Interactions of Binder with Silicon Particles and Electrolytes and Effects of Binders on Solid Electrolyte Interphase Formation. *ACS appl. mater. interfaces* **2016**, *8* (19), 12211-12220.

26. Markus, I. M.; Lin, F.; Kam, K. C.; Asta, M.; Doeff, M. M., Computational and Experimental Investigation of Ti Substitution in $Li_1(Ni_xMn_xCo_{1-2x-y}Ti_y)O_2$ for Lithium Ion Batteries. *J. Phys. Chem. Lett.* **2014**, *5* (21), 3649-3655.

27. Yin, W.; Alvarado, J.; Barim, G.; Scott, M. C.; Peng, X.; Doeff, M. M., A layered nonstoichiometric lepidocrocite-type sodium titanate anode material for sodium-ion batteries. *MRS Energy Sustain.* **2021**, *8* (2), 88-97.

28. Mahler, J.; Persson, I., A study of the hydration of the alkali metal ions in aqueous solution. *Inorg. Chem.* **2012**, *51* (1), 425-438.

29. Chen, K. Y.; Zhang, W. X.; Liu, Y.; Zhu, H. P.; Duan, J.; Xiang, X. H.; Xue, L. H.; Huang, Y. H., Carbon coated $K_{0.8}Ti_{1.73}Li_{0.27}O_4$: a novel anode material for sodium-ion batteries with a long cycle life. *Chem. Commun.* **2015**, *51* (9), 1608-1611.

30. Yin, W.; Barim, G.; Peng, X.; Kedzie, E. A.; Scott, M. C.; McCloskey, B. D.; Doeff, M. M., Tailoring the structure and electrochemical performance of sodium titanate anodes by post-synthesis heating. *J. Mater. Chem. A* **2022**, *10* (47), 25178-25187.

31. Rudola, A.; Saravanan, K.; Devaraj, S.; Gong, H.; Balaya, P., $Na_2Ti_6O_{13}$: a potential anode for grid-storage sodium-ion batteries. *Chem. Commun.* **2013**, *49* (67), 7451-7453.

32. Doeff, M. M.; Cabana, J.; Shirpour, M., Titanate Anodes for Sodium Ion Batteries. *J. Inorg. Organomet. Polym. Mater.* **2013**, *24* (1), 5-14.

33. Plashnitsa, L. S. K., E.; Noguchi, Y.; Okada, S; and Yamaki, J.-I., Performance of NASICON Symmetric Cell with Ionic Liquid Electrolyte. *J. Electrochem. Soc.* **2010**, *157* (4), A536-A543.

34. Barim, G.; Dhall, R.; Arca, E.; Kuykendall, T. R.; Yin, W.; Takeuchi, K. J.; Takeuchi, E. S.; Marschilok, A. C.; Doeff, M. M., Heterostructured Lepidocrocite Titanate-Carbon Nanosheets for Electrochemical Applications. *ACS Appl. Nano Mater.* **2021**, *5* (1), 678-690.

35. Song, X.; Li, X.; Shan, H.; Wang, J.; Li, W.; Xu, K.; Zhang, K.; Sari, H. M. K.; Lei, L.; Xiao, W.; Qin, J.; Xie, C.; Sun, X., V-O-C Bonding of Heterointerface Boosting Kinetics of Free-Standing $Na_5V_{12}O_{32}$ Cathode for Ultralong Lifespan Sodium-Ion Batteries. *Adv. Funct. Mater.* **2023**, *34* (5), 2303211.

36. Sasaki, T. K., F.; Iida, M.; Michiue, Y.; Takenouchi, S.; Yajima, Y.; Izumi, F.; Chakoumakos, B. C.; and Watanabe, M., A Mixed Alkali Metal Titanate with the Lepidocrocite-like Layered Structure. Preparation, Crystal Structure, Protonic Form, and Acid-Base Intercalation Properties. *Chem. Mater.* **1998**, *10*, 4123-4128.

37. Hou, J.; Zheng, Y.; Su, Y.; Zhang, W.; Hoshide, T.; Xia, F.; Jie, J.; Li, Q.; Zhao, Z.; Ma, R.; Sasaki, T.; Geng, F., Macroscopic and Strong Ribbons of Functionality-Rich Metal Oxides from Highly Ordered Assembly of Unilamellar Sheets. *J. Am. Chem. Soc.* **2015**, *137* (40), 13200-13208.